materials

MDPI

Article

Effect of TiB_2 Nanoparticle Content on the Microstructure and Mechanical Properties of TiB_2/Mg-4Al-1.5Si Composites

Jian Liu [1,*], Xiaogang Chen [2], Wuxiao Wang [2,*], Yu Zhao [2] and Na He [2]

[1] Faculty of Printing, Packaging Engineering and Digital Media Technology, Xi'an University of Technology, Xi'an 710054, China
[2] School of Material Science and Engineering, Xi'an University of Technology, Xi'an 710048, China
* Correspondence: liujian@xaut.edu.cn (J.L.); wangwuxiao@163.com (W.W.)

Abstract: Coarse primary and eutectic Mg_2Si phases were generally precipitated in Mg-Al-Si alloys during solidification at a low cooling rate, which tends to deteriorate the strength and ductility of magnesium alloys due to stress concentration. Different volume fractions of TiB_2 nanoparticles (1%, 3%, and 5%) were added to an Mg-4Al-1.5Si alloy to refine the coarse Mg_2Si phases based on a heterogeneous nucleation mechanism. The nanoparticles were incorporated and dispersed in the molten Mg alloys and by using semi-solid stirring followed by ultrasonic treatment (SSUT), and TiB_2/Mg-4Al-1.5Si composites were obtained. The effect of TiB_2 content on the microstructure and mechanical properties of the composites was studied. The results showed that the average size of primary Mg_2Si phases and α-Mg grains decreased as the TiB_2 content raised, the dendritic primary Mg_2Si phases were refined into polygonal shapes with smaller sizes, and the refined primary Mg_2Si phases were uniformly distributed in the alloys after adding 1 vol.% or 3 vol.% TiB_2 nanoparticles. As the TiB_2 content increased, the morphology of the eutectic Mg_2Si phases was modified from coarse Chinese characters to short rod or fine dot shapes. Vickers hardness and yield strength of the composites reached a maximum (153 HV and 90.9 MPa, respectively) when TiB_2 content was 5 vol.%, while the most superior ultimate tensile strength (142.4 MPa) and elongation (9.2%) were obtained when TiB_2 content was 3 vol.%, which were improved by 173.2%, 31.5%, 69.8%, and 187.5%, respectively compared with the Mg-4Al-1.5Si alloys.

Keywords: Mg matrix composites; Mg_2Si phases; TiB_2; microstructure; mechanical properties

Citation: Liu, J.; Chen, X.; Wang, W.; Zhao, Y.; He, N. Effect of TiB_2 Nanoparticle Content on the Microstructure and Mechanical Properties of TiB_2/Mg-4Al-1.5Si Composites. *Materials* **2023**, *16*, 2852. https://doi.org/10.3390/ma16072852

Academic Editor: Hajo Dieringa

Received: 7 March 2023
Revised: 25 March 2023
Accepted: 27 March 2023
Published: 3 April 2023

1. Introduction

Mg-Al-based alloys are the most used cast magnesium alloys due to their low cost, high strength, and good corrosion resistance [1]. However, their high-temperature strength and creep resistance deteriorate at a temperature above 120 °C due to the softening of the $Mg_{17}Al_{12}$ phase with low thermal stability (melting point is 437 °C) [2]. Mg-Al-Si series magnesium alloys not only possess excellent castability and low cost but also display good creep resistance at temperatures up to 150 °C due to the introduction of Mg_2Si precipitate phases, which has a high melting point (1085 °C), high hardness (4600 HV), and high strength (1670 MPa) [3–5]. Fine precipitated Mg_2Si phases can provide dislocation and grain boundary pinning [6]. However, at a low solidification rate, eutectic Mg_2Si phases with Chinese character shapes generally precipitate from Mg-Al-Si alloys, and when the Si content exceeds 1.38 wt.%, coarse dendritic primary Mg_2Si phases with sharp corners and edges may appear, which will cause stress concentration and become a crack source, thereby deteriorating the strength and ductility of the alloy [7]. Therefore, it is necessary to control the size, morphology, and distribution of the Mg_2Si phases to improve the comprehensive mechanical properties of these alloys [8–10].

It has been reported that the addition of some ex situ or in situ ceramic particles to aluminum alloys containing a Mg_2Si phase not only can refine and modify the Mg_2Si phases

based on heterogeneous nucleation mechanism but can also serve as a reinforcement, improving the mechanical properties. Li et al. [11] found that the addition of SiC nanoparticles can promote the heterogeneous nucleation of the eutectic Mg_2Si phase to reduce its size in the Mg_2Si/Al composite, and the shape was changed from a short strip to a dot shape. Zhao et al. [12] reported that, with the increase of the content of SiC particles from 5 wt.% to 10 wt.%, the morphologies of the primary Mg_2Si in an Al-Si-Mg alloy remained unchanged, and the size of the primary Mg_2Si phase decreased slightly. However, when SiC particle addition reached 15 wt.%, the primary Mg_2Si particulates changed partially from polygonal to quadrangular with a decrease in size from 50 μm to 30 μm. The disregistry between the (0001) crystal plane of TiB_2 and the (200) crystal plane of Mg_2Si is 4.64% (less than 5% critical value); hence, TiB_2 can theoretically be used as heterogeneous nuclei to refine the coarse Mg_2Si phases [13,14], and this has been verified by our previous studies [15]. Xiao et al. [16] found that TiB_2 particles can refine α-Mg grains in an AZ91 matrix, and as TiB_2 particles increased, the size of α-Mg grains in the obtained TiB_2/AZ91 composite decreased significantly. In addition, TiB_2 is considered one of the ideal reinforcements for magnesium matrix composites due to its high hardness, high melting point, and strong chemical stability [17]. Sun et al. [18] added TiB_2 microparticles to Mg-Li-Al alloys via stir casting and found that the main strengthening mechanism was grain refinement and the coefficient of thermal expansion mismatch. Compared with the micron-size particulate reinforcements or fibers, comparable or even superior mechanical properties can be achieved in the magnesium matrix nanocomposites by adding only a small number of nanoparticles [19,20]. The high volume fraction of nanoparticles can not only bring more heterogeneous nucleation sites for Mg_2Si phases and α-Mg but can also improve the yield strength of the composites based on the Orowan mechanism [21]. However, it is a great challenge to disperse the high-volume fraction of nanoparticles in a metal melt due to their attractive van der Waals force [22]. Hence, it is necessary to determine an optimum value by investigating the effect of TiB_2 content on the mechanical properties of the composites.

In the present work, TiB_2 nanoparticles with different volume fractions were incorporated into an Mg-4Al-1.5Si alloy and dispersed using SSUT. Mg matrix composites hybrid reinforced by TiB_2 nanoparticles, and in situ Mg_2Si particles were obtained (TiB_2/Mg-4Al-1.5Si composites), and the effects of TiB_2 content on the microstructure and mechanical properties of the composites were systematically investigated.

2. Experimental Procedures

The Mg-4Al-1.5Si (wt.%) Mg alloy ingot was provided by Shanxi Yinguang Huasheng Magnesium Industry Co., Ltd., Wenxi, China. TiB_2 nanoparticles with an average diameter of 50 nm were obtained from Shanghai Xiangtian Nanomaterials Co., Ltd., Shanghai, China. Three groups of TiB_2/Mg-4Al-1.5Si composites containing 1 vol.%, 3 vol.%, and 5 vol.% TiB_2 nanoparticles were fabricated by SSTU, respectively, with the following steps: a cylindrical crucible was heated to 700 °C by a resistance furnace, then the Mg alloy ingot was put into the crucible and kept for 50 min until the alloy was completely melted. Then, to incorporate these nanoparticles into the melt, the melt temperature was reduced to 635 °C in the semi-solid state, and the TiB_2 nanoparticles, wrapped with aluminum foil and preheated at 635 °C were, fed into the melt. The melt containing TiB_2 nanoparticles was mechanically stirred at 600 rpm for 5 min, during which the nanoparticles were sucked into the melt by axial flow and dispersed in the melt under shearing action [22]. The melt in the semi-solid state has a certain viscosity, which prevents the nanoparticles from floating or settling during the stirring [23]. After the mechanical stirring, the melt was rapidly heated to a liquid state at 720 °C again and subjected to ultrasonic treatment for 20 min (the ultrasonic frequency was 20 kHz, and the power was 1.8 kW), in which the nanoparticle aggregation was eliminated under a cavitation effect, and the nanoparticles were further dispersed under acoustic streaming [24]. The melting, stirring, and ultrasonic treatment was carried out under RJ-2 covering flux (32 wt.%~40 wt.%KCl-38 wt.%~46 wt.% $MgCl_2$-3 wt.%~5 wt.% CaF_2-5 wt.%~8 wt.% $BaCl_2$) and in the atmosphere of argon gas to prevent melt oxidation

and combustion. After slag removal, the melt was poured into a cylindrical mold of carbon steel. For convenience, the matrix alloy and the obtained composites with different volume fractions were denoted simply as M-AC, 1-COM, 3-COM, and 5-COM.

Specimens for microstructure observation and mechanical property tests were machined from the center of the cast ingot. After grinding and polishing, the metallographic specimens were etched with an acetic-picral reagent (5 mL acetic acid, 5 mL picric acid, 10 mL H_2O, and 100 mL ethanol) for 10–15 s. The microstructures of the samples were observed by using OLYMPUS GX71 optical microscope (OM). Ten micrographs were taken from each the metallographic specimen as statistical analysis samples, and the equivalent diameters (D) of the primary Mg_2Si phases in the alloy and the composites were determined using Image-Pro Plus 6.0 by Equation (1) [25]:

$$D = 2(A/\pi)^{1/2} \quad (1)$$

where A denotes the area of a single Mg_2Si. The grain size of α-Mg was measured by the mean linear intercept method. Microstructure characterization was done using a JSM-6700F scanning electron microscope (SEM, JEOL, Tokyo, Japan) equipped with an energy-dispersive spectrum (EDS). Phase identification was carried out using an XRD-7000 X-ray diffractometer (Shimadzu, Kyoto, Japan). Tensile tests were conducted on an HT-2402 material testing machine at room temperature and 0.8 mm/min, the gauge dimension of the dog-bone tensile specimens is 15 mm × 5 mm × 2 mm, and at least three specimens for each material were tested to ensure the reproducibility of data. The hardness testing was taken on an HV-120 Vickers hardness tester with a load of 49 N and a dwell time of 15 s. To quantitatively evaluate the distribution of primary Mg_2Si phases, ten metallographic photographs of different positions were selected from each material as analysis samples, the number of the primary Mg_2Si phases was counted by Image-Pro Plus 6.0, and their distribution uniformity was evaluated by the relative standard deviation (RSD) method. The microstructures were divided into 2 × 4 sub-areas in the field of view region, and the amount of Mg_2Si phases in each sub-area was counted. The standard deviation S was then determined by Equation (2):

$$S = \sqrt{\frac{\sum_{i=1}^{n} (x_i - \overline{x})^2}{n-1}} \quad (2)$$

where n denotes the number of sub-areas, x_i, and $\overline{x}$ represent the amount in the ith sub-area and the average amount of the primary Mg_2Si phases, respectively. The smaller the S value, the more uniform the Mg_2Si phases are distributed in the matrix.

3. Results and Discussion

3.1. Microstructures

Figure 1a shows the XRD diffraction patterns of the TiB_2/Mg-4Al-1.5Si composites with different content of TiB_2 nanoparticles (1 vol.%, 3 vol.%, and 5 vol.%). It can be seen from Figure 1a that the composites consist of α-Mg (JCPDS 04-0770), β-$Mg_{17}Al_{12}$ (JCPDS 73-1148), Mg_2Si phases (JCPDS 34-0458), and TiB_2 (JCPDS 35-0741). The diffraction peaks of TiB_2 (JCPDS 35-0741) in the XRD diffraction patterns indicate that the TiB_2 nanoparticles have been incorporated into the Mg alloys by SSUT, and no other new phases are found in the composites, indicating the TiB_2 nanoparticles are thermally stable in the molten Mg alloys. In addition, the diffraction peaks of α-Mg shift towards the lower diffraction angles with the increase of TiB_2 nanoparticle content, as shown in Figure 1b. According to Bragg's equation [26],

$$2d \sin\theta = \lambda \quad (3)$$

where λ is the length of the incident wave, d is lattice spacing, and θ is the angle between the incident light and the crystal planes (Bragg diffraction angle). The lattice spacing (d) of the α-Mg increases as the diffraction angles (2θ) decrease to maintain the equation. The

increase in the lattice spacing may be due to the heterogeneous nucleation of α-Mg on the TiB_2 nanoparticles.

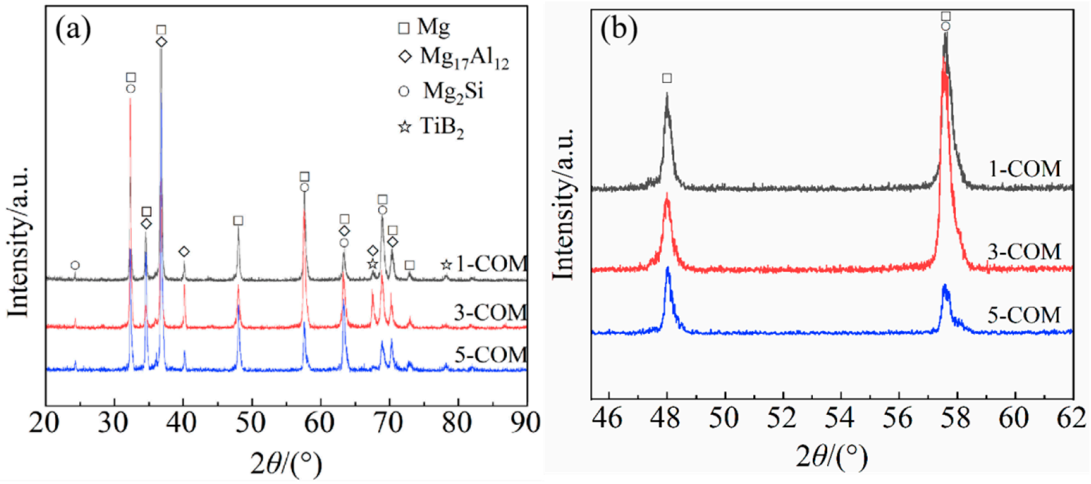

Figure 1. XRD patterns of TiB_2/Mg-4Al-1.5Si composites: (**a**) $20° \leq 2\theta \leq 90°$ and (**b**) $46° \leq 2\theta \leq 62°$.

Figure 2 shows the morphology and distribution of the primary Mg_2Si in the alloy and the composites. It can be found that the coarse dendritic primary Mg_2Si phases are nearly transformed into fine polygons as the TiB_2 content increases, as shown in Figure 2b–d. Figure 3 presents the size distributions of the primary Mg_2Si phases in the alloys and the composites. The average diameter of the primary Mg_2Si phases in the alloys is 70.74 μm, as shown in Figure 3a. The average diameter of the primary Mg_2Si phases decreases to 20.63 μm after adding 1 vol.% TiB_2 particles, and some particles are smaller than 10 μm in size, as shown in Figure 3b. When TiB_2 content rises to 3 vol.%, the average diameter of the primary Mg_2Si phases decreases to 17.56 μm, and the number of the primary Mg_2Si phases smaller than 10 μm in size increases, as shown in Figure 3c. When TiB_2 content reaches 5 vol.%, the average diameter of the primary Mg_2Si decreases to 15.21 μm, and there exists a small amount of primary Mg_2Si with a size less than 5 μm, while some primary Mg_2Si phases with size greater than 40 μm appear again, as shown in Figure 3d. The continuous decrease in the average diameter of the primary Mg_2Si phases with increasing TiB_2 content indicates that the TiB_2 nanoparticles significantly refined the primary Mg_2Si phases.

Figure 4 shows the *S* value in the alloy and the composites. It can be seen from Figure 4 that, after adding 1 vol.% and 3 vol.% TiB_2, the *S* value decreases from 7.64 to 3.43 and 3.22, respectively, while when TiB_2 content increases to 5 vol.%, the *S* value reaches 4.62 abnormally, indicating that the addition of 1 vol.% or 3 vol.% TiB_2 nanoparticles promoted the uniform precipitation of the primary Mg_2Si phases during solidification, and the deteriorated distribution uniformity may be associated closely with the dispersion of the TiB_2 nanoparticles in the 5-COM. It has been reported that when the addition of the TiB_2 nanoparticles exceeds 3 vol.%, it is challenging to disperse the nanoparticles since they tend to form clusters and segregate around grain boundaries during solidification [27,28], and these clusters and segregations are hard to entrap using the primary Mg_2Si phases. Hence, the distribution of the primary Mg_2Si phases in the 5-COM is poorer than that in the 1-COM and 3-COM.

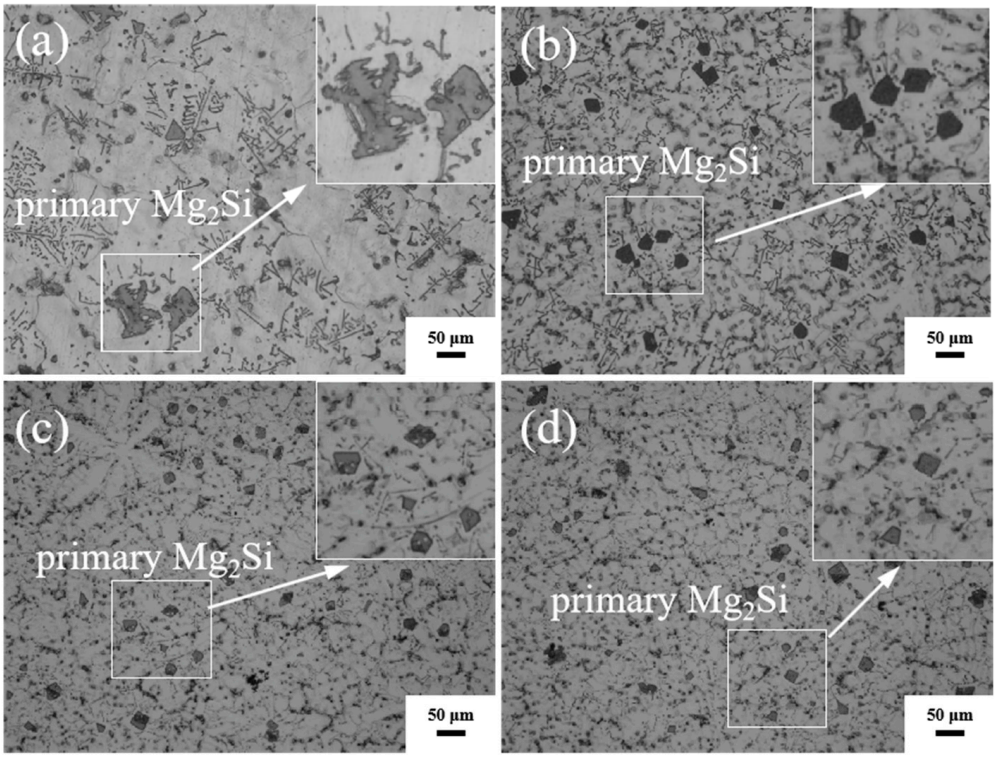

Figure 2. Optical micrograph of the alloys and composites, (**a**) M-AC, (**b**) 1-COM, (**c**) 3-COM, and (**d**) 5-COM showing the morphology and distribution of the primary Mg_2Si. (Scale bar = 50 μm).

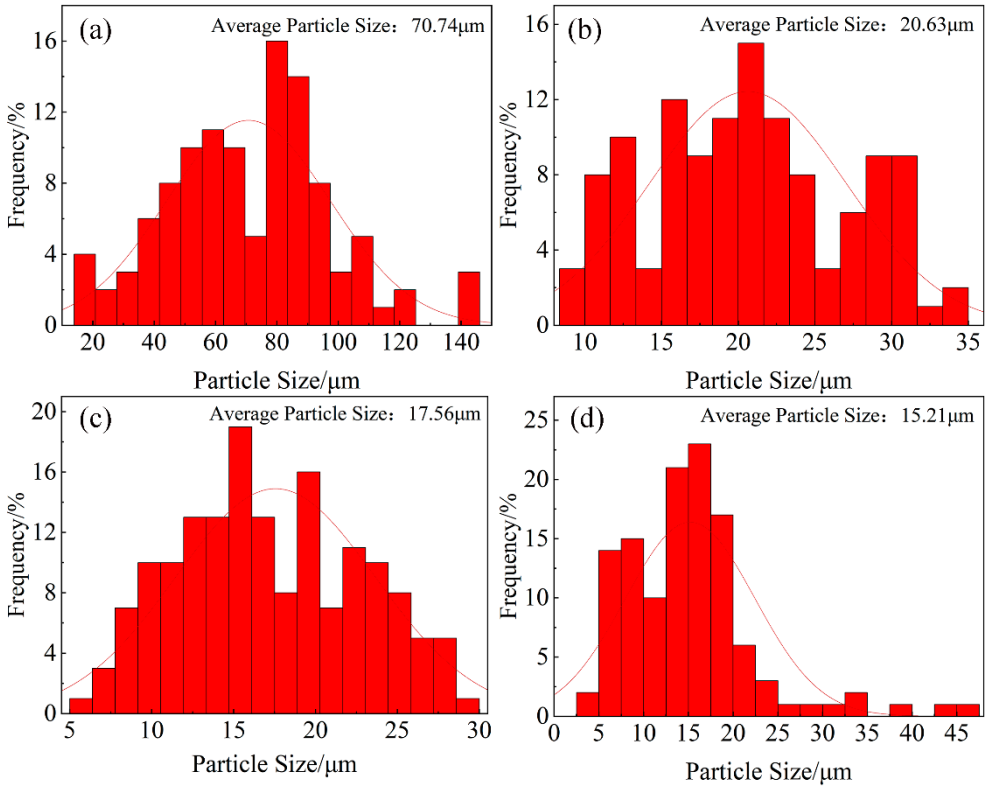

Figure 3. Size distributions of the primary Mg_2Si phases in the alloys and the composites, (**a**) M-AC, (**b**) 1-COM, (**c**) 3-COM, and (**d**) 5-COM.

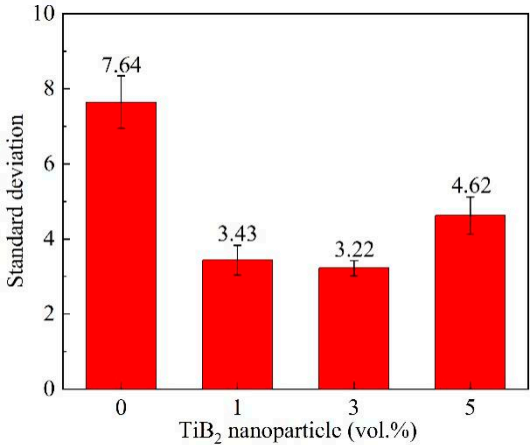

Figure 4. Standard deviation (*S*) of distribution uniformity of the primary Mg_2Si phases.

Figure 5 illustrates the morphology of the eutectic Mg_2Si phases in the alloy and the composites. The eutectic Mg_2Si phases in the M-AC mainly exhibit Chinese characters or long-rod shapes, as shown in Figure 5a. After adding 1 vol.% TiB_2 nanoparticles, a part of the eutectic Mg_2Si phases is transformed to the short rod type, as shown in Figure 5b. When TiB_2 content rises to 3 vol.%, the eutectic Mg_2Si phases with Chinese characters and short rod shapes are refined remarkably, as shown in Figure 5c. When the TiB_2 content reaches 5 vol.%, the eutectic Mg_2Si phases mainly exhibit a thin rod shape and a dot shape, as shown in Figure 5d. It can be inferred from Figure 5 that the TiB_2 nanoparticles also have a significant refining effect on the eutectic Mg_2Si phases in the magnesium alloys, and the refining effect becomes increasingly remarkable as the TiB_2 content escalates.

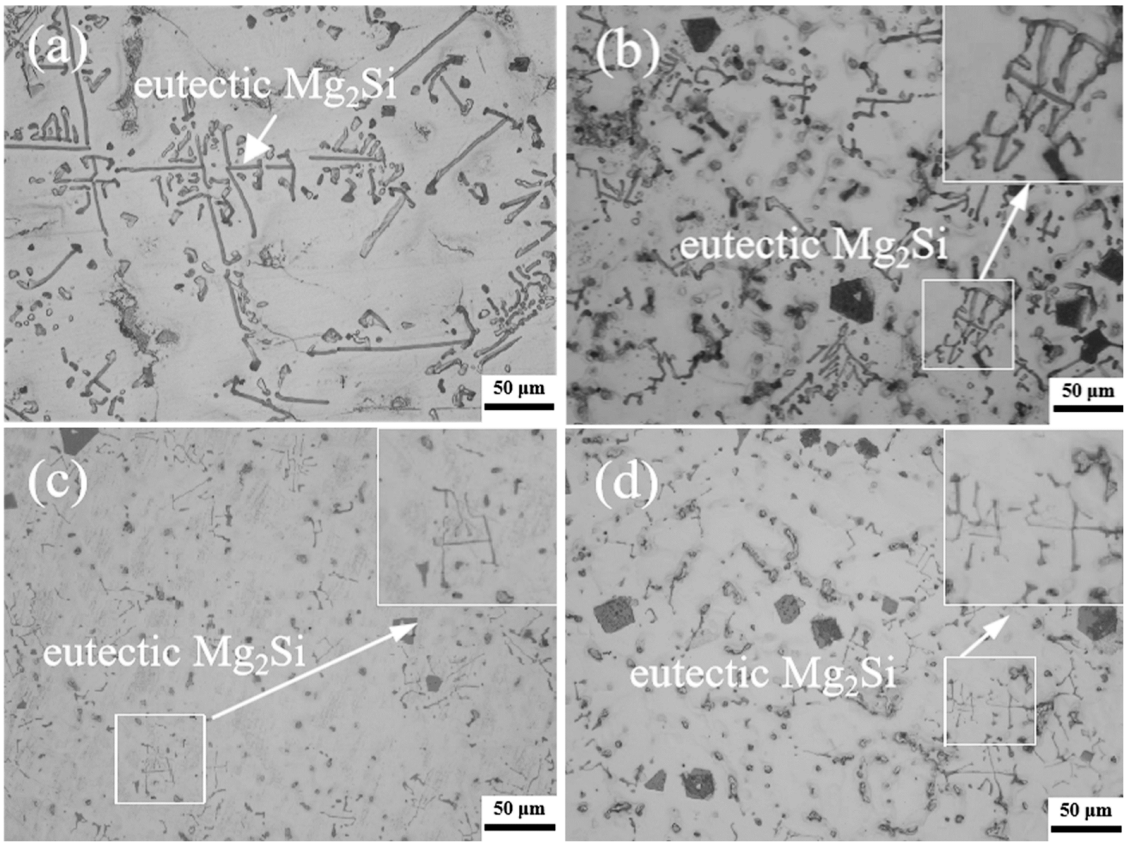

Figure 5. The morphologies of eutectic Mg_2Si in the alloy and the composites (**a**) M-AC, (**b**) 1-COM, (**c**) 3-COM, and (**d**) 5-COM. (Scale bar = 50 μm).

Figure 6 presents the microstructure of the alloys and the composites showing the morphology of α-Mg grains. Figure 7 illustrates the average size of α-Mg grain in the alloy and the composites with different content of TiB_2 nanoparticles. As shown in Figure 7, the average size of α-Mg grains in the alloys is about 219 μm. After adding 1 vol.% TiB_2, the average size of α-Mg grains is about 171 μm. When TiB_2 content is increased to 3 vol.%, the average size of α-Mg grains is about 161 μm. As the TiB_2 content rises to 5 vol.%, the average size of α-Mg grains is about 132 μm. When the content of the TiB_2 nanoparticles increases from 1 vol.% to 5 vol.%, the α-Mg grains are increasingly fine. The refinement of the α-Mg grains can be attributed to the following two aspects: first, the dispersed TiB_2 nanoparticles acted as heterogeneous nucleation sites for α-Mg grains to refine α-Mg grain size [16]; second, the TiB_2/Mg-4Al-1.5Si composite is an Mg matrix composite hybrid reinforced by TiB_2 nanoparticles and micro-scale in situ Mg_2Si phases, the TiB_2 nanoparticles and the refined Mg_2Si phases inhibited the growth of α-Mg grains. For the same volume fraction of reinforcement particles in metal matrix composites, smaller particles generally produce smaller grain sizes [29]. As the TiB_2 content rises, the average size of the primary Mg_2Si phases was reduced, and the fine primary Mg_2Si phases exhibited a more and more obvious inhibition role on the α-Mg grains consequently.

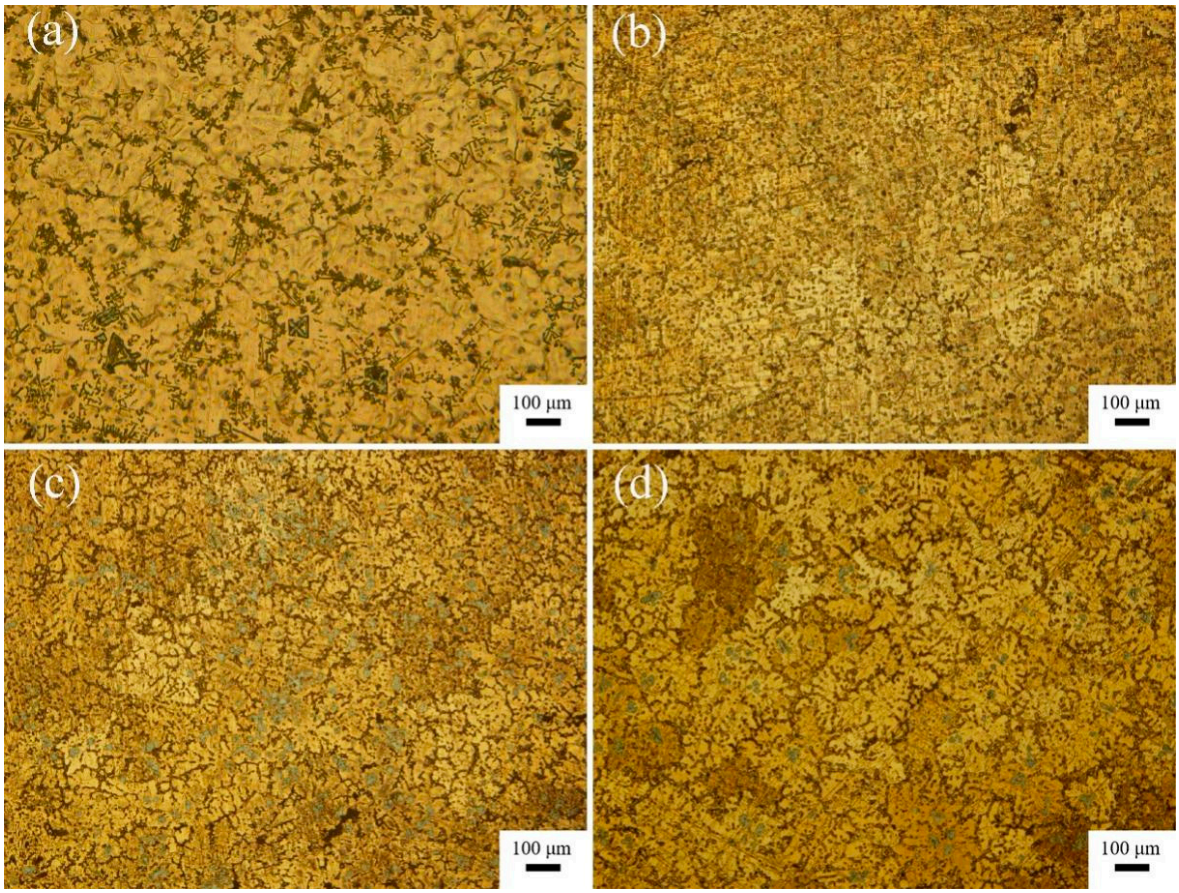

Figure 6. Metallographic photos of the alloys and composites showing the morphology of α-Mg grains: (**a**) M-AC, (**b**) 1-COM, (**c**) 3-COM, and (**d**) 5-COM.

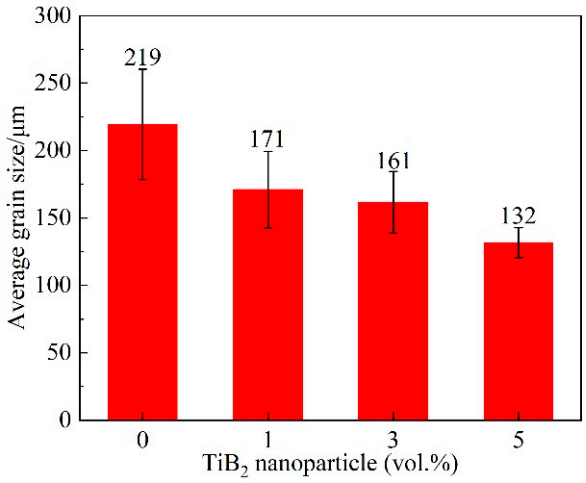

Figure 7. Variation of average grain size with vol.% of TiB_2 nanoparticles.

3.2. Mechanical Properties

Figure 8 shows the Vickers hardness of the alloys and the composites. It is seen that the hardness of the composites increases monotonically with the increase of TiB_2 content. When TiB_2 content is 5 vol.%, the hardness of the 5-COM reaches a maximum value of 153 HV, which is 173.2% greater than that of the matrix alloy. Figure 9 shows the engineering stress-strain curves of the alloys and the composites at room temperature, and the corresponding ultimate tensile strength (UTS), yield strength (YS), and elongation (EL) are listed in Table 1. UTS, YS, and EL of the TiB_2/Mg-4Al-1.5Si composites with different TiB_2 contents are higher than those of the matrix alloy. As the TiB_2 content rises, YS increases monotonically, while UTS and EL increase at first and then decrease, reaching a maximum when TiB_2 content is at 3 vol.%. The UTS, YS, and EL of the 3-COM are improved by 69.93%, 10.56%, and 187.5%, respectively, compared with the M-AC. When the TiB_2 content rises to 5 vol.%, the YS of the 5-COM is improved by 31.5%, but the UTS and EL decrease slightly. Therefore, it can be concluded that the strength and ductility of the Mg-4Al-1.5Si alloy can be simultaneously enhanced by adding an appropriate amount of TiB_2 nanoparticles, and desirable, comprehensive, mechanical properties can be obtained by adding 3 vol.% TiB_2 nanoparticles.

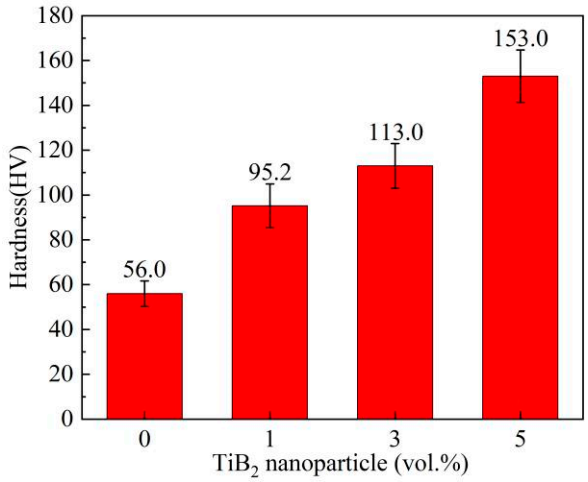

Figure 8. Variation of Vickers hardness with vol.% of TiB_2 nanoparticles.

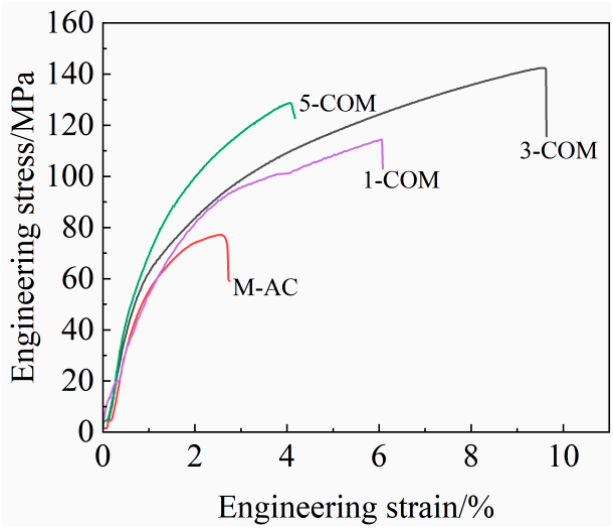

Figure 9. Typical tensile engineering stress-strain curves of the alloys and the composites.

Table 1. Mechanical properties of the alloys and the composites.

Materials	Hardness/HV	UTS/MPa	YS/MPa	EL/%
M-AC	56.0 ± 5.9	83.8 ± 14.1	69.1 ± 5.8	3.2 ± 0.8
1-COM	95.2 ± 9.7	108.8 ± 15.9	74.3 ± 11.7	5.1 ± 0.3
3-COM	113.0 ± 10.0	142.4 ± 11.4	76.4 ± 10.2	9.2 ± 1.1
5-COM	153.0 ± 11.7	125.3 ± 9.7	90.9 ± 9.3	3.4 ± 1.4

3.3. Strengthening and Toughening Mechanisms

The TiB_2/Mg-4Al-1.5Si composites exhibit greatly improved hardness and strength, which can be attributed to the following aspects: firstly, the TiB_2 nanoparticles and the refined Mg_2Si phases are both desirable reinforcements with high hardness and high modulus, which have a strong pinning effect on grain boundary and dislocation [13]. Secondly, smaller secondary particles generally possess higher fracture stress; hence, the refined Mg_2Si phases have a higher load-carrying capacity [30]. In addition, the average size of the α-Mg grain in the composites decreases with the addition of TiB_2 nanoparticles, and the grain refinement improves the YS of the composites according to the Hall–Petch relationship [31].

The improvement of ductility of the composites is mainly due to the refinement and homogeneous dispersion of the Mg_2Si phases. The primary Mg_2Si phases and the eutectic Mg_2Si phases in the M-AC exhibit a coarse, dendritic shape and a Chinese character shape, respectively, and the sharp tips and edges of the Mg_2Si phases provide an easy path for crack propagation, and the fracture path moves preferentially through these regions. Therefore, the EL of the Mg-4Al-1.5Si alloy is only 3.2%, as shown in Table 1. Figure 10 presents the fracture surfaces of the alloy and the composites. The fracture surface of the alloys is characterized by smooth cleavage planes, suggesting that it belongs to a brittle fracture mode (see Figure 10a). After adding 1 vol.% TiB_2 nanoparticles, the stress concentration level is decreased, and microcrack initiation is delayed due to the refinement and uniform distribution of the Mg_2Si phases, and the EL of 1-COM consequently increased to 5.1% (Table 1). As shown in Figure 10b, the area of the cleavage planes decreased in the fracture surface of the 1-COM, and a small number of dimples appeared on the fracture surfaces, which means it was a quasi-cleavage fracture mode. When the TiB_2 content rose to 3 vol.%, the Mg_2Si phases were further refined, and the distribution of the primary Mg_2Si phases was more uniform, which increased the compatible deformation capability of the composites, the EL of 3-COM consequently increased to 9.2% (Table 1). The fracture surfaces of the 3-COM were almost covered with a large number of small dimples, indicating the

dominant fracture behavior is a ductile fracture (see Figure 10c). When the TiB_2 content reached 5 vol.%, due to the relatively lower distribution uniformity of the primary Mg_2Si phases and the existence of large primary Mg_2Si phases in the 5-COM, the EL of 5-COM was only 3.4% (Table 1). Dimples and cleavage planes coexist in the fracture surface of the 5-COM, indicating that the fracture mode changed from ductile fractures to quasi-cleavage fractures again (Figure 10d).

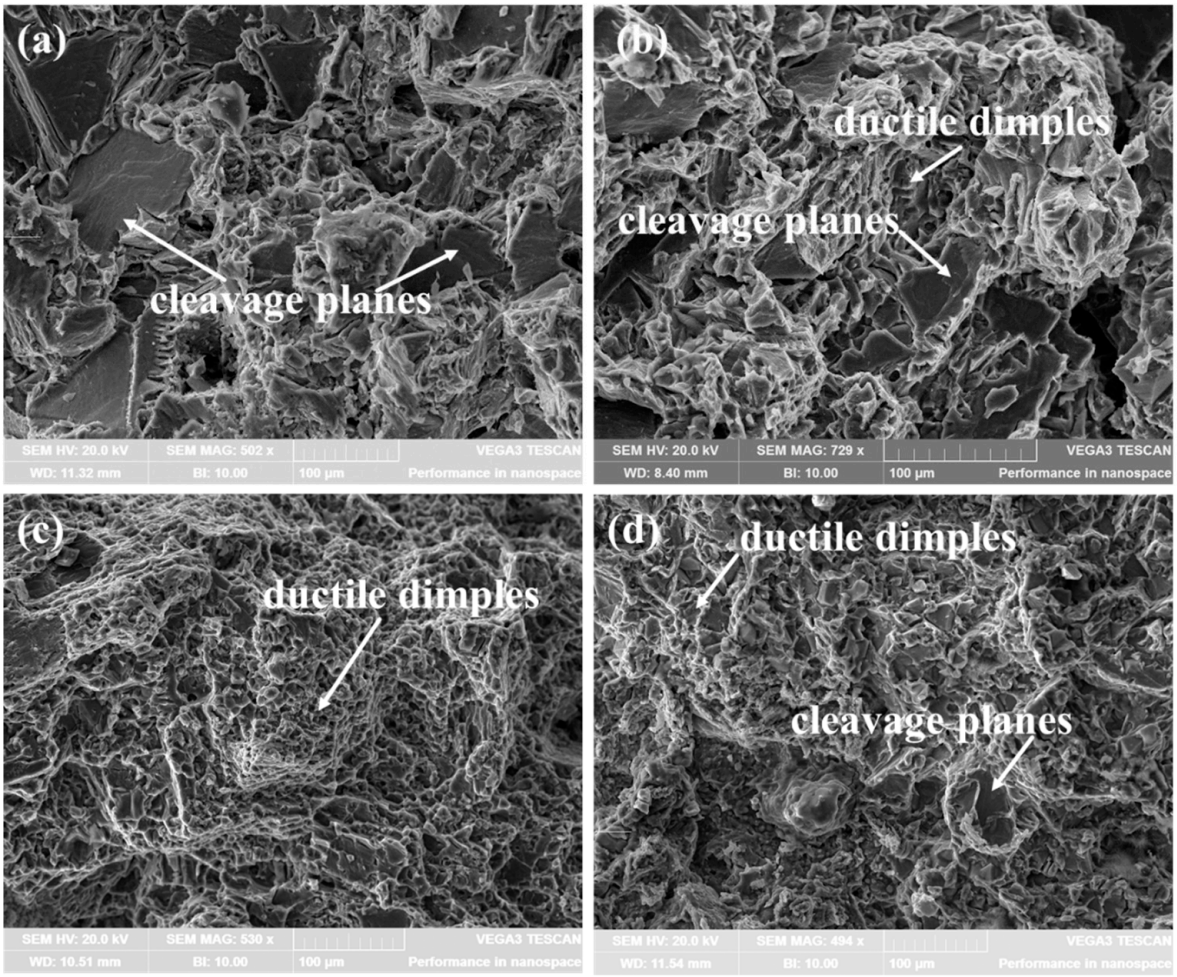

Figure 10. SEM images of fracture surfaces of the alloys and the composites: (**a**) M-AC, (**b**) 1-COM, (**c**) 3-COM, and (**d**) 5-COM.

4. Conclusions

The different volume fractions of TiB_2 nanoparticles (1%, 3%, and 5%) were incorporated into an Mg-4Al-1.5Si alloy by SSUT. Through microstructure observation and mechanical property testing, three main conclusions were drawn as follows:

(1) The TiB_2 nanoparticles not only refined the α-Mg grains but also refined the Mg_2Si phases in the composites. As the TiB_2 content increased, the average size of the α-Mg grains and the primary Mg_2Si phases decreased remarkably.

(2) When the content of the TiB_2 nanoparticles was 1 vol.% or 3 vol.%, the primary Mg_2Si phases were distributed uniformly in the Mg alloys, but the distribution uniformity decreased slightly when the TiB_2 content raised to 5 vol.%.

(3) As the TiB_2 content raised, the Vickers hardness and YS of the composites increased monotonically; the UTS and EL initially increased, followed by a decrease, reaching a maximum value when the TiB_2 content was 3 vol.%, achieving a synergistic improvement in strength and ductility.

Author Contributions: J.L.: Writing, reviewing, editing, and project administration. X.C.: Conceptualization, data curation, and writing—original draft; W.W.: Resources, supervision, and project administration; Y.Z.: Investigation; and N.H.: Software. All authors have read and agreed to the published version of the manuscript.

Funding: This work was supported by the National Nature Science Foundation of China (Program No. 52275377) and the Natural Science Basic Research Plan in Shaanxi Province of China in 2022 (Program No. 2022JM-236).

Institutional Review Board Statement: Not applicable.

Informed Consent Statement: Not applicable.

Data Availability Statement: Not applicable.

Conflicts of Interest: The authors declared no potential conflicts of interest to the research, authorship, and/or publication of this article.

References

1. Lin, X.P.; Dai, P.L.; Xu, C.; Fang, D.R.; Guo, K.Y.; Ren, Z. Solute redistribution and mechanism of structure refinement of Mg-Al alloy during solidification under high pressure. *J. Alloys Compd.* **2022**, *910*, 164777. [CrossRef]
2. Renhai, S. Nonisothermal dissolution kinetics on $Mg_{17}Al_{12}$ intermetallic in Mg-Al alloys. *J. Magnes. Alloy.* **2022**, *10*, 2421–2432.
3. Nakata, T.; Xu, C.; Sakai, T.; Miyamoto, T.; Liao, J.; Kamado, S. Effect of Si content on microstructures, tensile properties, and creep properties in a cast Mg-6Al-0.4Mn-2Ca(wt.%) alloy. *Mater. Sci. Eng. A* **2020**, *776*, 139018. [CrossRef]
4. Liu, Z.Q.; Jin, H.L.; Lai, Y.L.; Xia, Z.Y.; Li, G.B.; Guo, H.M.; Ding, J. The second phases of Mg-xAl-ySi-Ca alloys and their influences on properties. *Mater. Sci. Technol.* **2022**, *38*, 580–592. [CrossRef]
5. Pubo, L.; Yang, H.; Tan, W.T.; Gao, M.M. Effect of in situ Mg_2Si_p contents on microstructure and mechanical properties of Mg_2Si_p/AZ91D composites. *J. Mater. Sci.* **2021**, *56*, 6799–6813.
6. Hu, B.; Zhu, W.J.; Li, Z.X.; Lee, S.B.; Li, D.J.; Zeng, X.Q.; Choi, Y.S. Effects of Ce content on the modification of Mg_2Si phase in Mg-5Al-2Si alloy. *J. Magnes. Alloy.* **2021**, in press. [CrossRef]
7. Hu, T.; Wang, F.; Zheng, R.X.; Xiao, W.L.; Li, Y.; Lyu, S.Y.; Ma, C.L. Effects of B and Sn additions on the micro-structure and mechanical property of Mg-3Al-1Si alloy. *J. Alloys Compd.* **2019**, *796*, 1–8. [CrossRef]
8. Seth, P.P.; Parkash, O.; Kumar, D. Structure and mechanical behavior of in situ developed Mg_2Si phase in magnesium and aluminum alloys-a review. *RSC. Adv.* **2020**, *10*, 37327–37345. [CrossRef]
9. Chen, X.R.; Yin, Z.Y.; Le, Q.C.; Ning, S.C.; Yu, F.X. The microstructure refinement and strength enhancement of Mg-Al-Si alloy subjected by alternating-frequency ultrasonic melt treatment. *Int. J. Metalcast.* **2022**, *16*, 474–480. [CrossRef]
10. Zhang, X.P.; Zhang, Z.Y.; Wang, H.X.; Zhuang, Y.P.; Wang, L.F.; Cheng, W.L.; Liang, W. Synergistic effect of broken Mg_2Si and sub-micron $Mg_{17}Al_{12}$ induced by EX-ECAP on the strength and ductility of deformed Mg-4Al-1Si-1Gd alloy. *J. Mater. Res. Technol.* **2020**, *9*, 4230–4240. [CrossRef]
11. Li, J.Y.; Zhao, G.Z.; Wu, S.S.; Huang, Z.W.; Lü, S.L.; Chen, Q.; Li, F. Preparation of hybrid particulates SiC_{np} and Mg_2Si reinforced Al-Cu matrix Composites. *Mater. Sci. Eng. A* **2019**, *751*, 107–114. [CrossRef]
12. Zhao, Y.G.; Liu, X.B.; Yang, Y.Y.; Bian, T.J. Effect of SiC particle addition on microstructure of Mg_2Si/Al composite. *China Foundry* **2014**, *11*, 91–97.
13. Gao, Q.; Wu, S.S.; Lü, S.L.; Duan, X.C.; Zhong, Z.Y. Preparation of in-situ TiB_2 and Mg_2Si hybrid particulates reinforced Al-matrix composites. *J. Alloys Compd.* **2015**, *651*, 521–527. [CrossRef]
14. Du, R.; Du, Y.; Li, F.; Zhang, D.C.; Wu, S.S.; Lü, S.L. Effect of in-situ TiB_2 particles on microstructure and mechanical properties of Mg_2Si/Al composites. *J. Alloys Compd.* **2019**, *776*, 536–542. [CrossRef]
15. Wang, W.X.; Chen, X.G.; Liu, J.; Liu, D.C.; Liu, Z.Z.; Li, W.Z.; He, N. Effects of TiB_2 nanoparticles and ultrasonic vibration on the mechanical properties of an Mg-4Al-1.5Si alloy. *J. Alloys Compd.* **2022**, *912*, 165213. [CrossRef]
16. Xiao, P.; Gao, Y.M.; Xu, F.X.; Yang, S.S.; Li, B.; Li, Y.F.; Huang, Z.F.; Zheng, Q.L. An investigation on grain refinement mechanism of TiB_2 particulate reinforced AZ91 composites and its effect on mechanical properties. *J. Alloys Compd.* **2019**, *780*, 237–244. [CrossRef]
17. Xiao, P.; Gao, Y.; Yang, X.; Xu, F.X.; Yang, C.C.; Li, B.; Li, Y.F.; Liu, Z.W.; Zheng, Q.L. Processing microstructure and aging behavior of in-situ submicron TiB_2 particles reinforced AZ91 Mg matrix composites. *J. Alloys Compd.* **2018**, *764*, 96–106. [CrossRef]
18. Sun, J.W.; Ding, D.H.; Liu, W.C.; Wu, G.H.; Liu, H.J.; Wei, G.L.; Liu, H.Z. Strength and elastic modulus enhancement in Mg-Li-Al matrix composites reinforced by ex situ TiB_2 particles via stir casting. *J. Magnes. Alloy.* **2010**, *48*, 469–475. [CrossRef]
19. Xiao, P.; Gao, Y.M.; Yang, C.C.; Liu, Z.W.; Li, Y.F.; Xu, F.X. Microstructure, mechanical properties and strengthening mechanisms of Mg matrix composites reinforced with in situ nanosized TiB_2 particles. *Mater. Sci. Eng. A* **2018**, *710*, 251–259. [CrossRef]
20. Guan, H.T.; Xiao, H.; Ouyang, S.H.; Tang, A.; Chen, X.H.; Tan, J.; Feng, B.; She, J.; Zheng, K.H.; Pan, F.S. A review of the design, processes, and properties of Mg-based composites. *Nanotechnol. Rev.* **2022**, *11*, 712–730. [CrossRef]

21. He, H.Y.; Fan, G.L.; Saba, F.; Tan, Z.Q.; Su, Z.; Xiong, D.B.; Li, Z.Q. Enhanced distribution and mechanical properties of high content nanoparticles reinforced metal matrix composite prepared by flake dispersion. *Compos. Part B* **2023**, *252*, 110514. [CrossRef]
22. Tran, T.T.; Vo, T.T.; Cho, S.C.; Lee, D.H.; Hwang, W.R. A stir casting system for drawdown of light particles in manufacturing of metal matrix composites. *J. Mater. Process. Technol.* **2018**, *257*, 123–131. [CrossRef]
23. Chen, L.Y.; Peng, J.Y.; Xu, J.Q.; Choi, H.; Li, X.C. Achieving uniform distribution and dispersion of a high percentage of nanoparticles in metal matrix nanocomposites by solidification processing. *Scr. Mater.* **2013**, *69*, 634–637. [CrossRef]
24. Dieringa, H. Processing of magnesium-based metal matrix nanocomposites by ultrasound-assisted particle dispersion: A review. *Metal* **2018**, *8*, 431. [CrossRef]
25. Jin, Y.; Chen, G.; Zhang, X.; Chen, W.; Chen, T.; Ding, J.; Chang, Q.; Xie, Z.; Du, Z. Microstructures, mechanical properties and thixoformability of TiB_2/Al composite prepared by ultrasonic-assisted squeeze casting. *J. Mater. Eng. Perform.* **2022**, *31*, 9318–9330. [CrossRef]
26. Dong, Y.X.; Xiao, P.; Gao, Y.M.; Zhao, Q.Q.; Yang, H.C. Microstructure refinement and mechanical properties of eutectic Mg_2Si reinforced Mg matrix composites containing Sr element. *J. Mater. Res. Technol.* **2022**, *17*, 2614–2623. [CrossRef]
27. Gupta, M.; Wong, W.L.E. Magnesium-based nanocomposites: Lightweight materials of the future. *Mater. Charact.* **2015**, *105*, 30–46. [CrossRef]
28. Nie, K.B.; Wang, X.J.; Deng, K.K.; Hu, X.S.; Wu, K. Magnesium matrix composite reinforced by nanoparticles-a review. *J. Magnes. Alloy.* **2021**, *9*, 57–77. [CrossRef]
29. Ferguson, J.B.; Lopez, H.F.; Rohatgi, P.K. Impact of volume fraction and size of reinforcement particles on the grain size in metal-matrix micro and nanocomposites. *Metall. Mater. Trans. A* **2014**, *45*, 4055–4061. [CrossRef]
30. Yu, H.C.; Wang, H.Y.; Chen, L.; Zha, M.; Wang, C.; Li, C.; Jiang, Q.C. Spheroidization of primary Mg_2Si in Al-20Mg_2Si-4.5Cu alloy modified with Ca and Sb during T6 heat treatment process. *Mater. Sci. Eng. A* **2017**, *685*, 31–38. [CrossRef]
31. Sahoo, S.K.; Sahoo, B.N.; Panigrahi, S.K. Effect of in-situ sub-micron sized TiB_2 reinforcement on microstructure and mechanical properties in ZE41 magnesium matrix composites. *Mater. Sci. Eng. A* **2020**, *773*, 138883. [CrossRef]